Friction anisotropy at Ni(100)/(100) interfaces: Molecular dynamics studies

Yue Qi and Yang-Tse Cheng
GM R&D center, MC: 480-106-224, 30500 Mound Rd, Warren, Michigan 48090-9055

Tahir Çağin and William A. Goddard, III*
Material & Processing Simulation Center, 139-74, California Institute of Technology, Pasadena, California, 91125
(Received 8 March 2002; published 30 August 2002)

The friction of surfaces moving relative to each other must derive from the atomic interaction at interfaces. However, recent experiments bring into question the fundamental understanding of this phenomenon. The analytic theories predict that most perfect clean incommensurate interfaces would produce no static friction, whereas commensurate aligned surfaces would have very high friction. In contrast recent experiments show that the static friction coefficient between clean but 45° misoriented Ni(001) surfaces is only a factor of 4 smaller than for the aligned surfaces ($\theta \sim 0°$) and clearly does *not* vanish (θ is defined as the rotation angle between the relative crystallographic orientations of two parallel surfaces). To understand this friction anisotropy and the difference between analytic theory and experiment, we carried out a series of nonequilibrium molecular dynamics simulations at 300 K for sliding of Ni(001)/Ni(001) interfaces under a constant shear force. Our molecular dynamics calculations on interfaces with the top layer roughed (and rms roughness of 0.8 Å) lead to the static frictional coefficients in good agreement with the corresponding experimental data. On the other hand, perfect smooth surfaces (rms roughness of 0 Å) lead to a factor of 34–330 decreasing of static friction coefficients for misaligned surfaces, a result more consistent with the analytic theories. This shows that the major source of the discrepancy is that small amounts of roughness dramatically increase the friction on incommensurate surfaces, so that misaligned directions are comparable to aligned directions.

DOI: 10.1103/PhysRevB.66.085420 PACS number(s): 68.35.Af, 71.15.Pd

I. INTRODUCTION

Macroscopic friction follows Amonton's Law, which states that the frictional force f needed to slide one object laterally over another is proportional to the normal load F_n,

$$f = \mu_d F_n ,$$

where the constant, μ_d is the *dynamic friction coefficient*.[1] In addition, two solid bodies placed together in dry contact exhibit *static friction* in which no relative motion occurs until a threshold force is exceeded. The ratio of F_c, the force needed to initiate motion between objects at rest, and the load F_n is defined as the *static friction coefficient*,

$$F_c = \mu_s F_n .$$

However, the origin of this static friction is not well understood. Analytic theories indicate that static friction vanishes at most clean, *incommensurate* crystal interfaces due to the lack of periodicity, but it is quite large when clean surfaces are commensurate, when the surfaces deform elastically, and the interactions between the surfaces are weak.[2–5] These analytic models focus on such intrinsic factors as the interactions between constituent atoms, while ignoring such complicating factors as surface roughness, fracture, plastic deformation, and contaminants.

In a recent study of friction anisotropy at Ni(100)/Ni(100) interfaces Ko and Gellman[6] found that the static friction coefficient between two clean Ni(100) surfaces has a maximum of $\mu_s = 8.6 \pm 2.5$ when aligned and decreases monotonically to a minimum of $\mu_s = 2.5 \pm 1$ when the two surfaces are misoriented by 45°. Thus in contradiction with the analytic models, they observe a significant static friction at the misoriented interface; however, the reason for this anisotropy was not clear. This result differs from measurements on mica surfaces, where Hirano *et al.*[7] found that the friction force anisotropy depends strongly on the ''lattice misfit angle.''

Robbins *et al.* recently used molecular dynamics (MD) simulations to study the origin of static friction anisotropy, and proposed that the absorption of a ''third body,'' such as small hydrocarbon molecules, can cause the nonvanishing static friction between two macroscopic objects.[8] However, the model proposed by Robbins *et al.* cannot explain the experiments at Ni(001)/Ni(001) interfaces, because the experiments were carried out in a highly controlled ultrahigh vacuum (UHV) environment. These authors were careful to show that no impurities were present on the surface [as measured by Auger electron spectroscopy (AES)] and that the surfaces were well ordered (as measured by LEED). However, the Ni surfaces were polished mechanically and hence were not atomically flat.

In order to clarify the issues operating in the Ko and Gellman[6] experiments and to provide a better understanding of the origin of the friction anisotropy in dry sliding, including the effects of surface roughness, dislocation generation, and plastic deformation, we performed a series of nonequilibrium molecular dynamics (NEMD) simulations[9] for sliding of Ni(001) interfaces designed to mimic the experimental conditions. Section II describes the details of the calculations. We analyze the effect of surface roughness by comparing the differences in static friction coefficients for atomically flat and rough surfaces. These simulation results and comparison with experimental results are discussed in Sec. III.

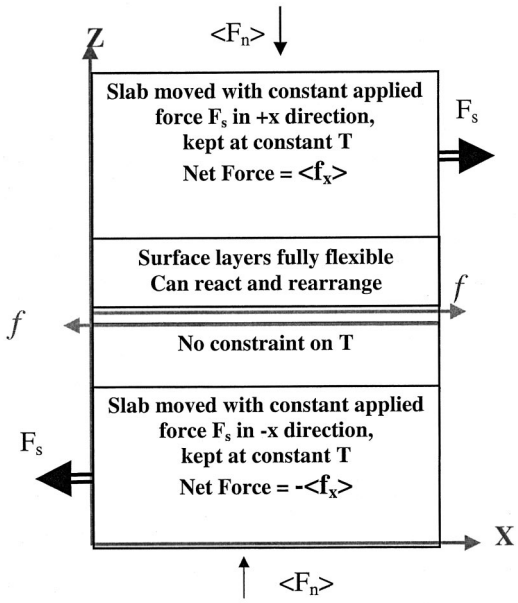

FIG. 1. Projection along the *y* direction of the 2D periodic cell (along the *x* and *y* directions) for the steady-state nonequilibrium molecular dynamics simulations. F_s is the applied external force on two moving slabs with 12 layers of atoms, *f* is the frictional force during the sliding of two slabs, and $\langle F_n \rangle$ is the normal load in the *z* direction.

II. SIMULATIONS

A. Calculation methods

We used the quantum modified Sutton-Chen (QMSC)-type many-body force field (FF) to describe the interactions of Ni atoms. The parameters for this FF (Ref. 10) were determined to match the experimental properties of bulk Ni (density, cohesive energy, compressibility, elastic constants, and phonon dispersion), including zero-point motion of lattice. This QMSC FF has previously been used to study structural transitions between various phases of Ni, Cu, and other face-centered-cubic (fcc) metals.[11–15]

The MD simulations considered finite thickness slabs (*z* direction) periodically infinite in the *x* and *y* directions. These ''samples'' were first prepared separately by equilibrating the upper and lower slabs of Ni for 20 ps at 300 K (0.001-ps time steps) using the Nose-Hoover thermostat with a relaxation constant of 0.1 ps and fixed volume molecular dynamics (ThN MD).[16,17]

The two slabs of Ni were then brought into contact and equilibrated for another 20 ps using ThN MD.

After equilibrating the sample, external forces were applied to simulate the sliding process. Figure 1 shows the *y* projection of the two-dimensional (2D) periodic cell (*x* and *y* periodic, and *z* nonperiodic) used for the steady-state NEMD sliding simulations. The *z* direction is along the (001) axis of Ni while the *x* and *y* directions were based on the orientations of the sliding experiments. All models considered 14 layers of (001) planes in each slab. At each time step, an external force of F_s, was applied along $+x$ direction for the top $N_r=12$ layers of atoms (termed a *moving slab*) and along the $-x$ direction for the bottom $N_r=12$ layers of atoms (a moving slab). The top layer in the top slab and the bottom layer in the bottom slab were constrained not to move in the *z* direction. This allowed us to simulate the sample under compression, keeping fixed the length of the sample along the *z* direction. The *interface zone*, consisting of two layers of atoms on each slab, was fully flexible and allowed to move freely (no external forces, no constraints, and no thermal damping).

The moving slabs were thermostated to a fixed temperature $T=300$ K (isokinetic energy). The atoms of the interface zone were subject to frictional heating and allowed to exchange energy with the rest of the slab through lattice vibrations. The averaged normal force per atom, $\langle F_n \rangle$, was calculated from the total compressive stress of the system averaged over the simulation time times the contact area then divided by the number of atoms. The average of the total lateral force on the top rigid slab per atom was calculated as $\langle f_x \rangle$, which was summed over all atoms of the top rigid slab and averaged over time and the number of atoms. This force is equal and opposite to the lateral force on the bottom rigid slab.

We increased the external force F_s until the two slabs started to slide with respect to each other. The minimum force needed to initiate motion is defined as F_c, and the static friction coefficient is defined as

$$\mu_s = F_c / \langle F_n \rangle, \tag{1}$$

where $\langle F_n \rangle$ is the averaged normal load.

After the two slabs start to move, the average atomic net forces $\langle f_x \rangle$ in the upper and lower slabs differ from the applied force. This difference is caused by the frictional force *f* at the interface. This frictional force is given by

$$f = F_s - \langle f_x \rangle. \tag{2}$$

The average acceleration in the *x* direction of each atom, caused by the net force $\langle f_x \rangle$ is given by $a = \langle f_x \rangle / m$, where *m* is the atomic mass. From the frictional force, the dynamic friction coefficient is calculated from Eq. (3),

$$\mu_d = f / \langle F_n \rangle. \tag{3}$$

The unit of force per atom is (kJ/mol)/nm$=1.6604 \times 10^{-12}$ N in this paper.

B. Orientations and mismatch angels

We examined the effect of orientation on both the dynamic and static coefficient of friction for three orientations of the two surfaces shown in Fig. 2:

- $\theta=0°$ case. In this case both surfaces are aligned. The direction of sliding is taken as the $\langle 110 \rangle$ direction for both slabs, the same as in the experiment. For each slab, the simulation cell size is $7\sqrt{2}a \times 7\sqrt{2}a \times 14a$ along the *x*, *y*, and *z* directions, respectively, while the total number of atoms *N* in the system is 5488 per periodic cell. This system is expected to have a very high coefficient of friction, particularly for the static friction of the perfectly smooth surface.
- $\theta=45°$ case, where the $\langle 110 \rangle$ axis of the lower surface matches the $\langle 100 \rangle$ direction of the top surface. In this case,

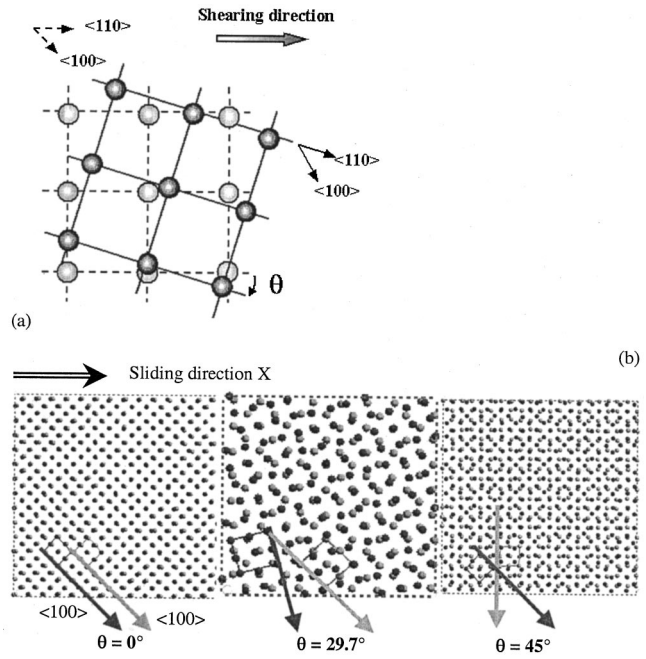

FIG. 2. (a) Schematic diagram showing the lattice mismatch of Ni(100) interfaces. (b) The *z* projection of the simulation cell. The dark circles are atoms of upper slab and light circles are atoms of lower slab. θ is the lattice misoriented angle between the upper and lower slabs. The sliding direction is along the *x* direction of the simulation cell.

the direction of sliding is taken as the $\langle 100 \rangle$ direction of the upper slab and $\langle 110 \rangle$ for the lower slab. Since periodic boundary conditions are applied along the *x* and *y* directions, the sizes for both slabs need to be equal along these two directions. To minimize the lattice mismatch, we choose $10a \times 10a \times 7a$ for the lower slab, and $7\sqrt{2}a \times 7\sqrt{2}a \times 7a$ for the upper slab, and then stretch the upper slab by 1% (tension strain) to reach $10a$ to match the periodicity in the lower slab. The total number of atoms in this system is 5544 per periodic cell.

• $\theta = 30°$ case (actually $\theta = 29.7°$). In this case, the sliding direction is the $\langle 1\ 1\ 0 \rangle$ orientation for the lower slab and the $\langle \bar{3}\ 11\ 0 \rangle$ orientation for the upper slab. To minimize lattice mismatch, we choose $4\sqrt{2}a \times 4\sqrt{2}a \times 7a$ for the lower slab and $\sqrt{130}a/2 \times \sqrt{130}a/2 \times 7a$ for the upper slab, and then compress the upper slab by 0.7% (compression strain) to reach the same length as the lower slab. The number of atoms in the simulation cell is 1806 per periodic cell. We also doubled the cell length in both directions, such that the simulation cell is 7224 atoms, and the cell size did not change our results.

To obtain the same sliding conditions as used in the experiment, the sliding direction is always along the *x* direction and the lattice misorientation angle is kept constant during each sliding simulation.

C. Surface roughness

We constructed two surface structures, including flat and rough surfaces, for each orientation.

• The perfect interface, where each surface is atomically flat. When the surfaces are aligned ($\theta = 0°$), the sliding corresponds to slip inside a single crystal. This surface has an rms roughness of 0 Å.

• The random rough interface, where 25% of the atoms in the interface zone are randomly deleted from each surface (thus for the $\theta = 0°$ case, we eliminated 49 of the 196 atoms in the top layer of each surface). This surface has an rms roughness of 0.8 Å.

This paper considers only random rough interface models in detail, and we will include different rough surface configurations in the future studies.

III. RESULTS AND DISCUSSION

We studied smooth and random rough surfaces for $\theta = 0°$, 45°, and 30° as summarized in Table I. The applied force F_s, net atomic force $\langle f_x \rangle$, friction force *f*, and normal force $\langle f_n \rangle$ were defined as in Sec. II A. The relative displacement of the center of mass of each slab was tracked during the MD simulations and used to calculate the center of mass velocity and acceleration along the *x* direction.

A. Perfect interfaces ($\theta = 0°$ and $\theta = 45°$)

Figure 3 shows the relative displacement in the *x* direction between upper and lower slabs for the Ni(001)/Ni(001) atomically flat interface under a constant external force F_s. Figure 3(a) is for the perfect alignment case ($\theta = 0°$), and Fig. 3(b) is for the $\theta = 45°$ misorientation case.

For $\theta = 0°$ we observe oscillatory motion of two slabs for $F_s \leqslant 15$, indicating that the two slabs are *not* sliding with respect to each other. But for $F_s \geqslant 20.17$ the slabs do slide. Therefore $15 < F_c \leqslant 20.17$.

For the $\theta = 45°$ misorientation case there is no such oscillation for $F_s < 0.255$, indicating that $0.05 < F_c \leqslant 0.255$. Clearly, for a perfect surface the friction at the misoriented interface is only ~1% of that for the aligned interface ($\theta = 0°$).

Figure 4 shows the snapshots of the atomic structure of the corresponding interfaces whose sliding behaviors are plotted in Fig. 3. Figure 4(a) is for the perfect alignment ($\theta = 0°$) case with an applied force of $F_s = 20.17$ after 5 ps and Fig. 4(b) is for the $\theta = 45°$ misorientation case with $F_s = 0.255$ after 10 ps. We note here that the misoriented surface has essentially no damage, whereas the aligned surface already exhibits some damage. These results for the perfect surfaces are consistent with the expectations of the analytic theories.

B. Rough interfaces ($\theta = 0°$ and $\theta = 45°$)

Figure 5 shows the relative displacement in the *x* direction between the upper and the lower slabs for the Ni(001)/Ni(001) random rough interface. Figure 5(a) for perfect alignment ($\theta = 0°$) shows oscillatory motion for $F_s = 10$ or lower, but sliding for $F_s = 12.6$ and higher, indicating that $10 < F_c \leqslant 12.6$. For the $\theta = 45°$ misorientation case the range of the critical force is $0.5 < F_c \leqslant 2.2$. Thus for the rough surface the ratio of the critical force of misoriented versus

TABLE I. Summary of results from NEMD simulations of friction at Ni(100)/Ni(100) interfaces. (The unit for force is kJ/mol$=1.66\times10^{-12}$ N the unit for velocity is Å/ps$=100$ m/s, and the unit for acceleration is Å/ps$^2=10^{14}$ m/s^2.)

Orientation	Applied F_s	$\langle fx\rangle$	Friction $f=F_s-\langle fx\rangle$	$\langle fn\rangle$ obtained from stress	Velocity or acceleration	Friction coefficients μs or μd
$\theta=0°$; flat	5.04	0		0	$v=0$	
	15.13	0.07	15.13	0.55	$v=0$	
	20.17	3.035	17.14	2.95	$a=0.09$ $2\langle fx\rangle/m=0.10$	$\mu s\cong6.84$
	25.2	7.59	17.61	6.36	$a=0.246$ $2\langle fx\rangle/m=0.258$	$\mu d=2.77$
$\theta=0°$; rough	5.04	0	5.04	0.52	$v=0$	
	10.08	0	10.08	0.89	$v=0$	
	12.6	0.62	11.98	1.43	$v=0.1$	$\mu s=8.80$
	15.13	3.32	11.81	2.71	$a=0.12$ $2\langle fx\rangle/m=0.11$	$\mu d=4.35$
	25.2	9.2	16	3.97	$a=0.35$ $2\langle fx\rangle/m=0.31$	$\mu d=4.03$
$\theta=30°$; flat	0.029	0	0.029		$v=0$	
	0.057	0.006	0.051	2.55		$\mu s=0.022$
	0.144	0.104	0.04	2.7		$\mu d=0.015$
	0.288	0.105	0.183	2.85		$\mu d=0.065$
$\theta=30°$; rough	1.44	0	1.44		$v=0$	
	2.88	0	2.88		$v=0$	
	4.32	0.15	4.17	0.65		$\mu s=6.65$
	5.76	0.26	5.5	0.77		$\mu d=7.15$
$\theta=45°$; flat	0.05	0	0.05	1.20	$v=0$	
	0.255	0.130	0.125	1.19	$v=0.082$	$\mu s=0.21$
	0.509	0.273	0.236	1.21	$a=0.009$ $2\langle fx\rangle/m=0.009$	$\mu d=0.19$
	2.55	1.31	1.24	1.23	$a=0.0487$ $2\langle fx\rangle/m=0.045$	$\mu d=1.01$
	5.09	2.96	2.13	1.22	$a=0.111$ $2\langle fx\rangle/m=0.101$	$\mu d=1.75$
$\theta=45°$; rough	0.509	0	0.509	1.28	$v=0$	
	2.55	0.06	2.49	1.24	$v=0.25$ m/s	$\mu s=2.06$
	5.09	0.75	4.34	1.52	$a=0.025$ $2\langle fx\rangle/m=0.026$	$\mu d=2.85$

aligned surfaces is ~17.8%, compared to ~1.26% for the perfect flat surfaces. Clearly surface roughness dramatically increases (by a factor of 14) the ratio of the critical force for the $\theta=45°$ misorientation case and that for the $\theta=0°$ case.

Figure 6 shows snapshots of the atomic structure of the rough interfaces whose sliding behaviors are plotted in Fig. 5. Figure 6(a) is the structure for perfect alignment ($\theta=0°$) with $F_s=12.6$ after 6 ps and Fig. 6(b) is the snapshot for $\theta=45°$ misorientation with an applied force of $F_s=2.25$ after 10 ps. In both cases, the rough interface leads to disordering. For the perfect alignment case the plastic deformation and disordering generated at the interface propagates into the bulk of each slab however for the $\theta=45°$ misoriented interface the plastic deformation was more localized on the surface layers.

C. Deformation at commensurate interfaces

In the perfect alignment case ($\theta=0°$), we observed that the two slabs of materials collapse into one when brought to a spacing below a critical distance. This ''adhesion avalanche'' phenomenon was previously predicted for Ni(001) using the equivalent crystal method.[18]

For the perfect alignment case, sliding is equivalent to shearing of a perfect crystal, leading to very high ''friction.'' Experiments conducted under similar conditions lead to cold welding. That is the shearing force was so large that it approached the upper limit of the tribometer. Thus for the case of perfect alignment ($\theta=0°$), sliding requires generating dislocations and other defects to accommodate plastic deformation at the interface. This results in a rough interface [Fig.

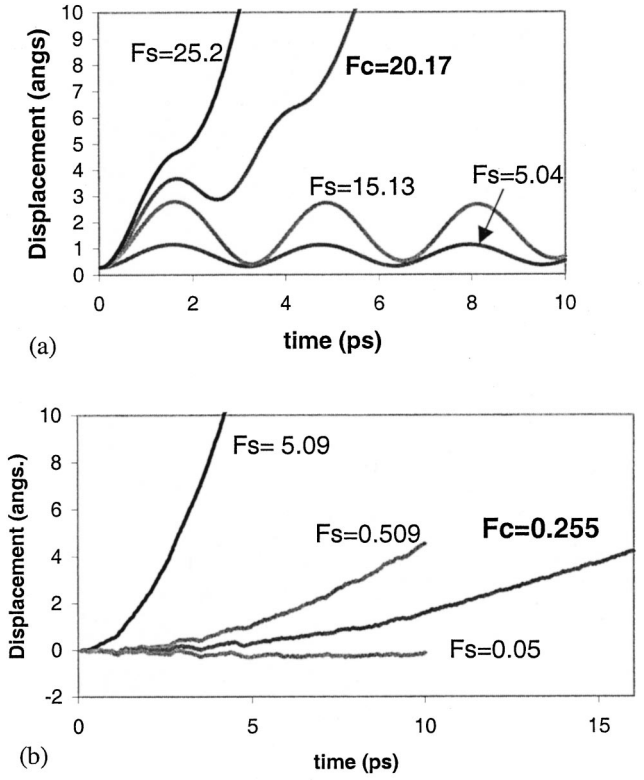

FIG. 3. Relative displacement in the x direction between the upper and lower slabs for Ni(100)/Ni(100) perfect flat interfaces. (a) The $\theta=0°$ aligned case, $F_c=20.17$; (b) the $\theta=45°$ misorientation interface, $F_c=0.255$.

4(a)]. In contrast, for the misaligned case ($\theta=45°$) the interface remains atomically flat during sliding with no dislocation generation observed.

We found that for perfect alignment ($\theta=0°$), both flat and rough surfaces lead to pronounced oscillatory motion between the slabs when the external force is below F_c. For

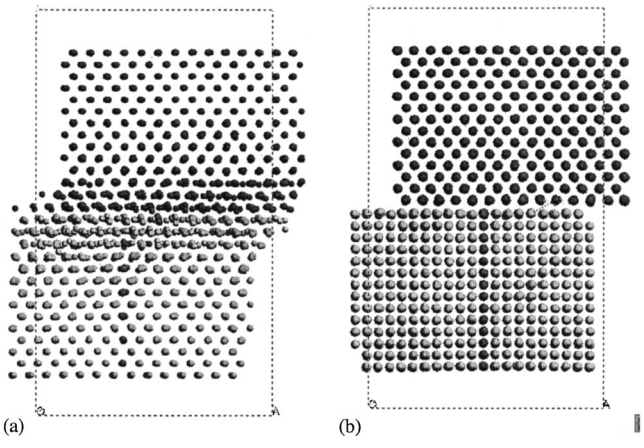

FIG. 4. Snapshots of the atomic structure of the Ni(100)/Ni(100) interfaces after sliding. (a) perfectly flat with perfect alignment ($\theta=0°$) after an applied force of $F_s=20.17$ for 5 ps; (b) perfectly flat with $\theta=45°$ misorientation after an applied force of $F_s=0.255$ for 10 ps.

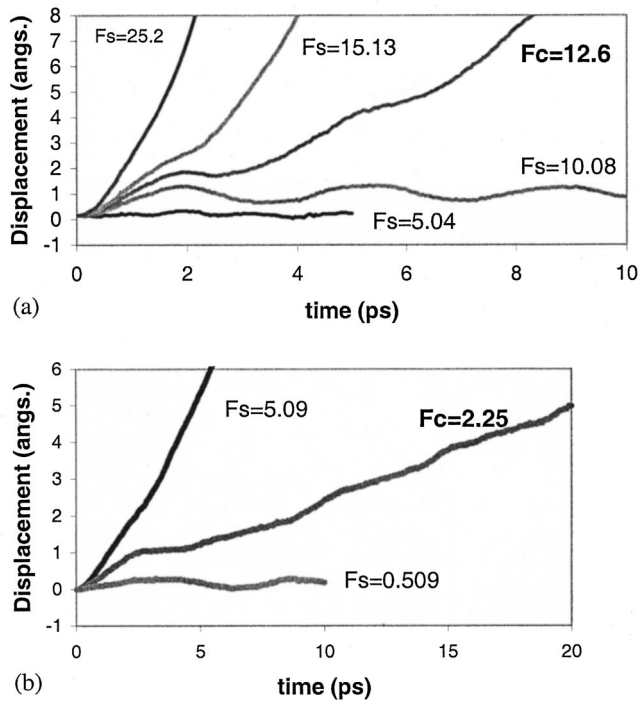

FIG. 5. Relative displacements in the x direction between the upper and lower slabs for Ni(100)/Ni(100) rough interface (rms roughness of 0.8 Å). (a) for $\theta=0°$ aligned case, $F_c=12.6$ and (b) for $\theta=45°$ misorientation interface, $F_c=2.25$.

the misoriented $\theta=45°$ case we also observe oscillatory motion but since F_c is quite small the oscillations are not large.

As the applied force increases to the critical force F_c, we observe a barrier at the beginning of sliding (similar to the first peak in the oscillation) for the aligned $\theta=0°$ case but not in the misoriented $\theta=45°$ case. This indicates that sliding is intermittent rather than smooth. This phenomena is similar to the experimental observations of ''stick-slip'' behavior in $\theta=0°$ sliding, but only slip motion in $\theta=45°$ sliding.[6]

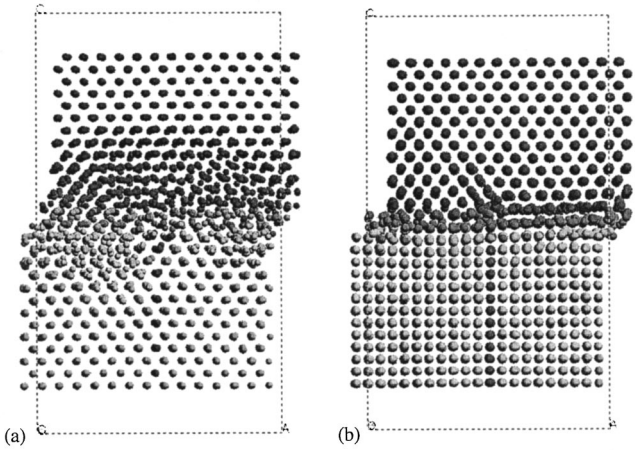

FIG. 6. Snapshots of the atomic structure of the Ni(100)/Ni(100) rough interfaces after sliding. (a) perfect alignment ($\theta=0°$) after an applied force of $F_s=12.6$ for 6 ps and (b) $\theta=45°$ misorientation after an applied force of $F_s=2.25$ for 10 ps.

The barrier in sliding for the aligned $\theta=0°$ interface suggests the existence of energy minima or ''lock positions'' leading to the stick-slip motion. Even for the rough interface the underlying periodic lattices of the upper and lower slabs are commensurate, leading to multiple minima. For the misoriented $\theta=45°$ interface, the lack of commensurateness between the upper and lower slabs (except that of the supercell) works against the presences of such a lock position so that slip motion is generally observed.

To understand the process of stick slip, we analyzed the atomic trajectories in detail. For forces less than the critical force [$F_s=15.13$ and $F_s=5.04$ in Fig. 3(a)] and before the displacement reaches the peak (up to 1.6 ps), the whole upper slab of Ni is elastically sheared with respect to the lower slab (uniform displacement with time). This is followed by a decrease in displacement (1.6–3.2 ps) due to the release of the accumulated elastic shear strain. When the applied force is larger than the critical force [$F_s=20.17$ for Fig. 3(a)], only pure elastic deformation is observed before the first peak ($0\sim1.6$ ps), then plastic deformation starts to occur at the interface (1.6–2.0 ps), which then leads to a continuous increase in the relative displacement (2–10 ps). This demonstrates that plastic deformation is necessary for sliding, whereas elastic deformation is responsible for the ''stick'' motion. Li *et al.* showed that elastic deformation of the surface layers is the main cause for the stick-slip phenomenon in Ni-Al alloy.[19] They also observed the ''stick-slip'' phenomena at incommensurate interfaces. In contrast, we observe only ''slip'' at incommensurate interfaces. However, our mechanism for the stick-slip behavior is consistent with their observations.

For the perfectly aligned case, we estimated the critical shear stress from the critical force for sliding. This leads to a critical stress between 4.875 GPa (for $F_s=15.13$) and 6.5 GPa (for $F_s=20.17$). The critical stress for sliding is related to the theoretical shear strength of Ni. Using the experimental tetragonal shear modulus for Ni (Ref. 20) of $\gamma=35$ GPa (the calculated value from our force field is 49.6 GPa), leads to a critical shear between $\gamma/5.4$ to $\gamma/7$, which is close to the theoretical strength predicted by Frenkel's model.[21]

The relative displacement of two slabs in perfectly aligned cases oscillated at a frequency. We found out that the oscillation frequency does not depend on the magnitude of the applied force, the number of layers with F_s being applied, nor the length of the simulation cell along x or y directions. However, if the total length of slabs along the z direction is doubled, the frequency doubles. This indicates that the frequency is related to the time of sound velocity traveled along the z direction.

D. Comparison with experimental results

The calculated values of the static friction coefficient are compared with the experimental observations of Ko and Gellman in Fig. 7. The MD simulation results of both static friction coefficients and their anisotropy behavior as a function of misorientation angle for rough interfaces agree well with the experimental. Therefore we believe that surface roughness and interface disordering are the main causes for the experimentally observed anisotropic behavior of at the Ni(001)/Ni(001) interfaces.

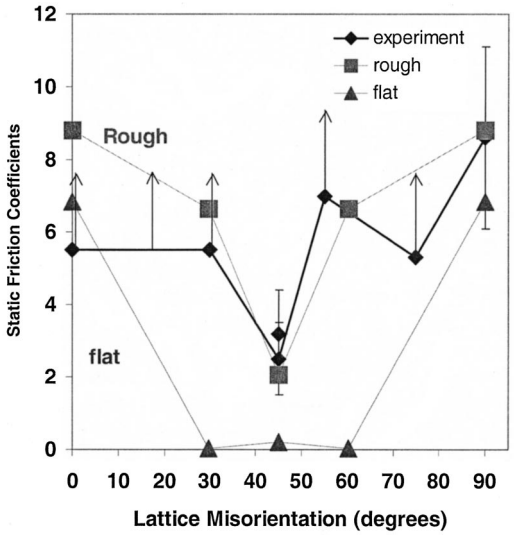

FIG. 7. Static friction coefficients as a function of the lattice misorientation angle between two Ni(100) surfaces. The experimental values measured by Gellman and Ko are shown with solid diamonds, where the points with upward arrows represent the lower limit from the experiment. The solid square symbols indicate simulation results for rough interfaces (0.8-Å rms). These values are in excellent agreement with experiment. The solid triangles static indicate simulation results for atomically flat interfaces.

For the MD calculations with rough interfaces, the static frictional coefficients are

$$\mu_s=8.8 \text{ for } \theta=0°,\ \mu_s=6.65 \text{ for } \theta=30°,$$

$$\text{and } \mu_s=2.06 \text{ for } \theta=45°.$$

The corresponding experimental data were

$$\mu_s=8.6\pm2.5 \text{ for } \theta=0°,\ \mu_s=5.5\pm2 \text{ for } \theta=30°,$$

$$\text{and } \mu_s=2.5\pm1.0 \text{ for } \theta=45.$$

Thus the simulation results for random rough interface agree very well with the experimental data.

In contrast, MD simulations with atomically flat interfaces lead to static frictional coefficients of

$$\mu_s\sim6.8 \text{ for } \theta=0°,\ \mu_s\sim0.02 \text{ for } \theta=30°,$$

$$\text{and } \mu_s\sim0.21 \text{ for } \theta=45°.$$

For the aligned case μ is comparable to the values for the rough surface obtained with MD and with the value from experiment. However, the static friction coefficients on perfect misoriented interfaces (for both $\theta=30°$ and $\theta=45°$) are much lower: a factor of 10 for $\theta=45°$ and a factor of 330 for $\theta=30°$. This shows a strong dependence on the misorientation angle θ. This anisotropic behavior agrees well with the analytic theories,[2–5] which conclude that there is no static friction on most clean incommensurate interfaces. Because

we used a supercell with periodic boundary condition in our simulation, there is a long-range ordering of the interface which could account for the small but nonzero static friction for the 30° and 45° cases, and for the dramatic differences between these two cases.

The MD simulations show that roughness in only the top layer or two of the surface is necessary to account for the experimental observation that the static friction coefficients varies by less than a factor of 4 for various orientations. The similar values for perfect and rough aligned surfaces arise because even just 5 ps of MD is sufficient to roughen the surface [see Fig. 4(a)]. We observed that only ~1 Å of roughness is sufficient to lead to the observed anisotropy in roughness. Thus to achieve a large ratio in friction anisotropy (say a factor of 10–100) would probably require a roughness of less than 1 Å, which would be very difficult to achieve experimentally. Both theory and experimental agree that there is a minimum static friction coefficient occurs for $\theta = 45°$.

IV. SUMMARY

We describe an approach for using molecular dynamics simulations to elucidate the phenomena resulting in friction at metal surfaces. We illustrated this approach by simulating the friction behavior of Ni(001)/Ni(001) interfaces as a function of crystal orientation. The results show that just 1 Å of surface roughness dramatically increases the static friction coefficients of clean, incommensurate Ni interfaces.

Allowing just one monolayer of roughness, the MD simulation results of static friction coefficients agree well with the experimental observation of Ko and Gellman both in the magnitude and in their anisotropy as a function of misorientation angle. This explains the discrepancy concerning the anisotropic behavior of the friction coefficient between analytical theories of friction and the experimental observation of Ni(001)/Ni(001) interfaces.

ACKNOWLEDGMENTS

We want to thank Professor Andy Gellman for alerting us to his work prior to publication. This work was carried out at both GM and the Materials and Processing Simulation Center (MSC) at Caltech. The facilities of the MSC are supported by grants from DOE-ASCI-ASAP, NSF (CHE9985574), ARO-MURI, Chevron, 3M, Seiko Epson, GM, Avery Dennison, Beckman Institute, Asahi Chemical, and Nippon Steel.

*Author to whom correspondence should be addressed. Email address: wag@wag.caltech.edu

[1] B. N. J. Persson, *Sliding Friction, Physical Principles and Applications* (Springer, New York, 1998).

[2] Y. I. Frenkel and T. Kontorova, Zh. Eksp. Teor. Fiz. **8**, 1340 (1938); K. Shinjo and M. Hirano, Surf. Sci. **283**, 473 (1993).

[3] M. O. Robbins and E. D. Smith, Langmuir **12**, 4543 (1996).

[4] S. Aubry, *Solitions and Condensed Matter Physics*, Springer Series in Solid State Sciences Vol. 8, edited by A. R. Bishop and T. Schneider (Springer-Verlag, Berlin, 1978).

[5] T. Strunz and F. J. Elmer, Phys. Rev. E **58**, 1601 (1998); A. Vanossi *et al.*, *ibid.* **63**, 017203 (2001).

[6] J. S. Ko and A. J. Gellman, Langmuir **16**, 8343 (2000).

[7] M. Hirano, K. Shinjo, R. Kaneko, and Y. Murata, Phys. Rev. Lett. **67**, 2642 (1991).

[8] G. He, M. H. Muser, and M. O. Robbins, Science **284**, 1650 (1999).

[9] W. A. Goddard, III, T. Çağin, Y. Qi, Y. Zhou, and J. Che, in *Tribological Research: From Model Experiments to Industrial Problems*, edited by G. Dalmar, A. A. Lubrecht, D. Dowson, and M. Priest (Elsevier, Amsterdam, 2001), p. 15–33.

[10] T. Cagin, Y. Qi, H. Li, Y. Kimura, H. Ikeda, W. L. Johnson, and W. A. Goddard, III, *Bulk Metallic Gasses*, edited by W. L. Johnson, C. T. Liu, and A. Inoue Mater. Res. Soc. Symp. Proc. No. 554 (Materials Research Society, Pittsburgh, 1999), p. 43.

[11] Y. Qi, T. Cagin, Y. Kimura, and W. A. Goddard, III, Phys. Rev. B **59**, 3527 (1999).

[12] Y. Qi, T. Cagin, W. L. Johnson, and W. A. Goddard, III, J. Chem. Phys. **115**, 385 (2001).

[13] Y. Qi, H. Ikeda, T. Cagin, K. Samwer, W. L. Johnson, and W. A. Goddard, III; *Bulk Metallic Glasses* (Ref. 10) p. 367.

[14] H. Ikeda, Y. Qi, T. Cagin, K. Samwer, W. L. Johnson, and W. A. Goddard, Phys. Rev. Lett. **82**, 2900 (1999).

[15] Y. Qi, A. Strachan, T. Cagin, and W. A. Goddard, III, Mater. Sci. Eng., A **309**, 156 (2001).

[16] W. G. Hoover, Phys. Rev. A **31**, 1695 (1985).

[17] Yue Qi, Ph.D. thesis, Caltech, 2001; see also Y. Qi, T. Cagin, W. A. Goddard, III, J. Comput-Aided Mater Des (to be published).

[18] J. R. Smith, G. Bozzolo, A. Banerjea, and J. Ferrante, Phys. Rev. Lett. **63**, 1269 (1989).

[19] B. Li, P. C. Clapp, J. A. Rifkin, and X. M. Zhang, J. Appl. Phys. **90**, 3090 (2001).

[20] J. P. Hirth and J. Lothe, *Theory of Dislocation*, 2nd Ed. (Krieger, Malabar, 1992).

[21] J. Frenkel, Z. Phys. **37**, 572 (1926).